Mechanical Testing and Diagnosis
ISSN 2247 – 9635, 2012 (II), Volume 2, 5-14

NANOMECHANICAL TESTING OF HYDROGEN EFFECTS ON SUPER DUPLEX STAINLESS STEEL

Adina BASA [1], Afrooz BARNOUSH [2], Christian THAULOW [1]

[1] NTNU, Department of Engineering Design and Materials, Trondheim, NORWAY,
[2] Saarland University, Department of Material Science, Saarbruecken, GERMANY

adina.basa@ntnu.no , a.barnoush@matsci.uni-sb.de

ABSTRACT

The effect of hydrogen on the mechanical properties of the super duplex stainless steel is examined using in situ electrochemical nanoindentation (ECNI) tests. Within the ECNI, which is a nanoindenter combined with an electrochemical setup, the nanoindentation can be made on a surface that is immersed in an electrolyte and in situ electrochemically charged with hydrogen. In situ electrochemical nanoindentation testing captures the change in the onset of plasticity (pop-in load level) as well as the change in the hardness due to the absorption of the atomic hydrogen.

Keywords: Nanoindentation, hydrogen, duper duplex stainless steel, pop-in

1. INTRODUCTION

Over the last years, the interaction of steels with hydrogen has led to many incidents, sometimes causing catastrophic failures. The main sources for hydrogen are the corrosion from the aqueous solutions, the cathodic protection and the contaminants in the melting and welding processes. Different mechanisms for hydrogen have been proposed, but the most established ones are Hydrogen Enhanced Decohesion (HEDE) and Hydrogen Enhanced Local Plasticity (HELP). The HEDE mechanism (the brittle fracture) suggests that the hydrogen accumulated within the atomic lattice reduces the cohesive bonding strength and it was first proposed by Troiano [1]. The HELP mechanism (the ductile fracture) proposes that the atomic hydrogen enhances the mobility of the dislocations causing a lowering in the shear strength and it was described for the first time by Birnbaum and Sofronis [2].

The Super Duplex Stainless Steel (SDSS) is a widely used material in offshore applications due to its high strength and toughness and excellent corrosion resistance [3] given by the two phases, austenite (γ) and ferrite (α). The non-magnetic ductile austenite has a Faced-Centred Cubic (FCC) structure and it is acting like a crack stopper while the ferrite is more brittle due to its Body-Centred Cubic (BCC) structure. Despite these strong points, SDSS has often failed due to the hydrogen released during the cathodic protection leading to the hydrogen embrittlement. The main diffusion mechanism for hydrogen in

steel is the lattice diffusion by the interstitial jumps. The higher packing density of the austenite (0.74 as compared to 0.68 of the ferrite) [4] and its close packed lattice structure gives a higher solubility of the hydrogen atoms and a lower diffusion rate, while the ferrite is characterized by a higher diffusion rate and a lower solubility due to its open lattice structure. Although the concentration of hydrogen may be higher in the austenite, the ferrite is prone to the crack propagation at lower hydrogen concentration [5]. Even though many experimental studies [6, 7] and simulations [8, 9] of the hydrogen effect on SDSS have been done, a more complete understanding of the micro-mechanism is needed. A starting point for that is to provide a better characterization of the hydrogen effect on each individual phase and this can be done by the nanoindentation in combination with an electrochemical setup described below.

The nanoindentation is a widely used method [10,11] for studing the micromechanical properties of the materials. Recently, Barnoush et al. [12, 13] used the nanoindenter in combination with an electrochemical setup to investigate the effect of hydrogen on the micromechanical properties of different materials under hydrogen charging conditions. This is a promising method because the immediate effect of hydrogen on the local material microconstituents can be observed. Another advantage of using in-situ ECNI is related to the testing time, which is considerably lowered and limited to some hours while the nanoindentations are performed. Also, another big advantage is that the surface quality remains the same during testing, while in the case of ex-situ ECNI, either the surface is damaged [14] by the hydrogen during the long time charging or the hydrogen diffuses out of the material while the sample is transferred in between the electrochemical setup and the nanoindenter [15]. In-situ ECNI method is used in this paper and the authors would like to mention that the aim of this paper is primarily to describe the experimental procedure and to present only some preliminary results.

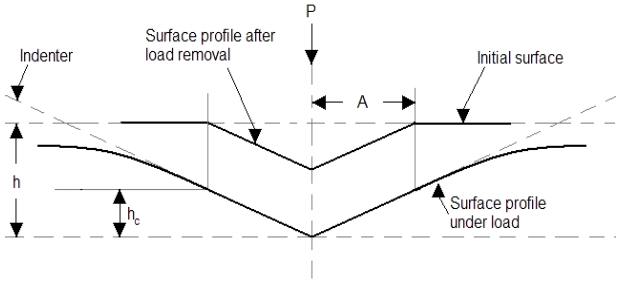

Fig. 1. The cross-sectional area of a nanoindentation

During a nanoindentation, an indenter tip is forced into the sample with a defined load. The maximum force is kept constant for a few seconds and then decreased, see Fig. 1. A load – displacement curve is produced, see **Fout! Verwijzingsbron niet gevonden.**, which is used to calculate the hardness and the reduced modulus of elasticity.

Three-sided pyramidal tips are standard for the nanoindentations [16]. The standard three-sided tip is the Berkovich tip, which has a total included angle from plane to edge of 142.3° and a half angle, θ, of 65.35°, see Fig. 3.

The hardness is calculated according to:

$$H = \frac{P_{max}}{A_c} \tag{1}$$

where P_{max} - the maximum applied load, A_c - the contact area, calculated from the tip area function, based on the contact depth, h_c.

Mechanical Testing and Diagnosis, ISSN 2247 – 9635, 2012 (II), Volume 2, 5-14

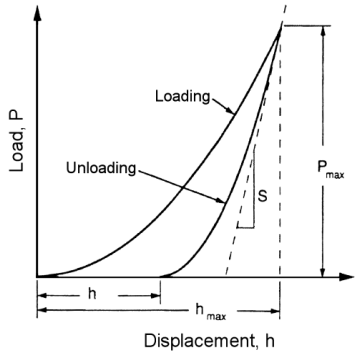

Fig. 2. Load – displacement curve produced during the nanoindentation

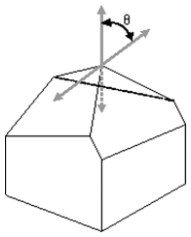

Fig. 3. Three-sided pyramidal Berkovich tip

For a perfect Berkovich indenter [10]:

$$A_c = 24.5 h_c^2 \tag{2}$$

$$h_c = h_{max} - \varepsilon \frac{P_{max}}{S} \tag{3}$$

where h_{max} - the maximum displacement, ε - the geometric constant equal to 0.75, S - the stiffness of the material.

In reality, an indenter tip will never be perfect, so, each tip will be calibrated according to its own tip area function. The procedure involves performing a series of 25 up to 100 indents of different contact depths (varying the loading levels) on a fused quartz sample with a know reduced modulus of 69.6 GPa. The contact area will be determined by measuring the stiffness based on the following equation:

$$A_c = \frac{\pi}{4}\left(\frac{S}{E_r}\right)^2 \tag{4}$$

where: E_r - the reduced modulus of elasticity.

Then, the contact area will be plotted as a function of the contact depth and the points will be fitted to a sixth order polynomial:

$$A_c = C_0 h_c^2 + C_1 h_c + C_2 h_c^{1/2} + C_3 h_c^{1/4} + \\ + C_4 h_c^{1/8} + C_5 h_c^{1/16} \tag{5}$$

where: C_0 - equal to 24.5 for a Berkovich tip, C_1 to C_5 - the curve fitting parameters.

The reduced modulus of elasticity is calculated as:

$$E_r = \frac{\sqrt{\pi}}{2}\frac{S}{\sqrt{A_c}} \tag{6}$$

The relation between the reduced modulus and the elastic modulus is:

$$\frac{1}{E_r} = \frac{1-\nu_s^2}{E_s} - \frac{1-\nu_i^2}{E_i} \tag{7}$$

where: ν - the Poisson ratio for the sample, respectively, the indenter; E - the elastic modulus of the sample, respectively, the indenter.

For a standard diamond indenter tip $E_i = 1140GPa$ and $\nu_i = 0.07$.

Mechanical Testing and Diagnosis, ISSN 2247 – 9635, 2012 (II), Volume 2, 5-14

2. EQUIPMENT AND SAMPLE PREPARATION

The experiments were performed with a Hysitron TriboScan TI-750 with Performech controller in combination with an electrochemical setup as shown in Fig. 4. A diamond Berkovich long tip, specially designed for testing inside the electrolyte was used. The used load function is presented in Fig. 5, where the last segment of 1 second holding time at 10% peak value was added for the drift correction.

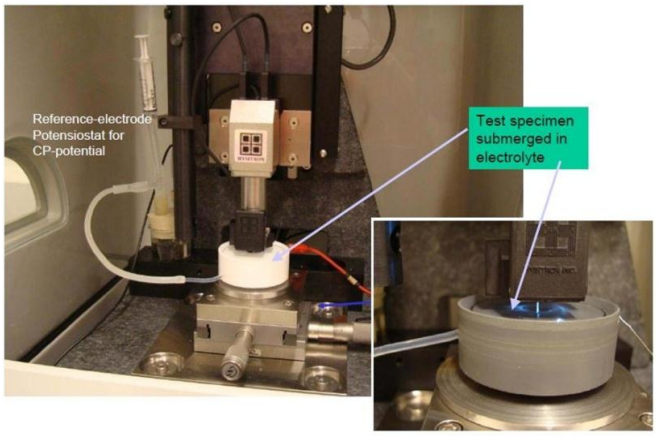

Fig. 4. The electrochemical setup

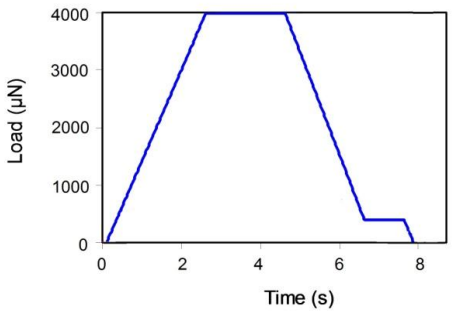

Fig. 5. Load function

As a counter electrode for the electrochemical setup, a platinum wire was used while a Saturated Calomel Electrode (SCE) was the reference electrode. The sample holder allows the sample to be covered with the electrolyte during testing.

A coarse grained SDSS with a chemical composition of 0.016% C, 0.46% Mn, 0.24% Si, 0.024% P, 0.001% S, 7.16% Ni, 25.22% Cr, 3.76% Mo, 0.276% N, 0.205% Cu and a Pitting Resistance Equivalent Number (PRE_N) equal to 42.044 has been investigated. The high pitting resistance is given by the high levels of chromium, molybdenum and nitrogen, as is calculated according to:

$$PRE_N = \%Cr + 3.3 \times \%Mo + 16 \times \%N \quad (8)$$

The macroscopic yield strength for this material is 560 MPa and the tensile strength is 790 MPa. These excellent properties are given by the dual phase microstructure of the austenite (γ) and ferrite (α), Fig. 6.

Mechanical Testing and Diagnosis, ISSN 2247 – 9635, 2012 (II), Volume 2, 5-14

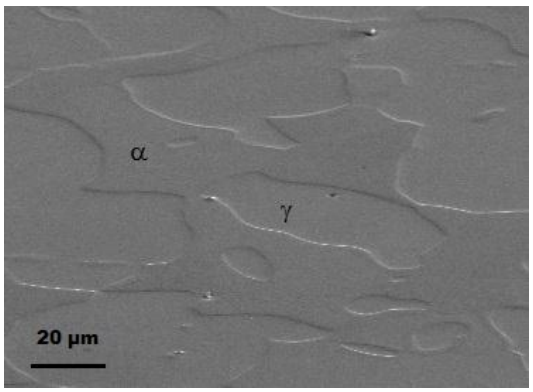

Fig. 6. SEM image of the coarse grained super duplex stainless steel

The starting point for the sample preparation was the grinding with silicon-carbide papers of grade 500, 1000 and 2400, followed by a mechanical polishing with a water based diamond suspension of 3 µm and 1 µm. The last step was the electropolishing in order to remove the work hardened microscopic leyer of the material caused by the mechanical polishing. Table 1 presents the electrolyte and the used electropolishing parameters [14].

Table 1. Parameters used for the electropolishing

Electrolyte	Pot., V	Flow rate	Time, s	Temp., °C
Methanol/H_2SO_4	15	8	15	21

The surface quality after the electropolishing is presented in Fig. 7. The Average Roughness (RA) is less than 10 nm, as given by the nanoindenter software.

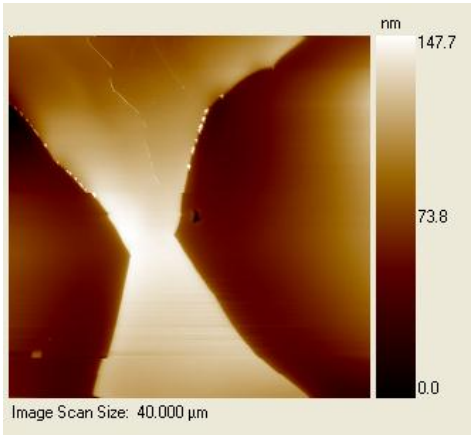

Fig. 7. Topography image, scanned with TI-750 prior testing, where the ferrite is light and the austenite is dark

3. EXPERIMENTAL RESULTS

Freshly electropolished samples were tested first in air and then in a 0.05 M Na_2SO_4 electrolyte. Hydrogen started to form when a cathodic potential of -1150 mV was applied.

Both the austenite and the ferrite phases were tested with a maximum load of 4000 μN and a loading rate of 2000 μN/s. Fig. 8 and Fig. 9 present the effect of hydrogen on the hardness and on the reduced modulus of elasticity, respectively.

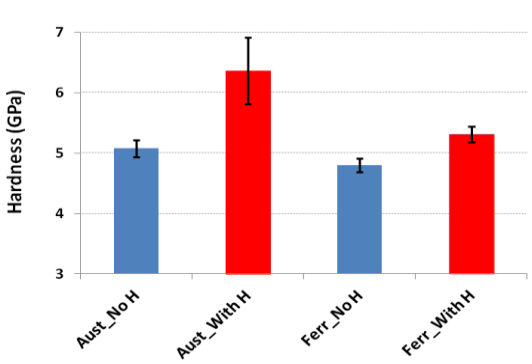

Fig. 8. The hydrogen effect on the sample hardness

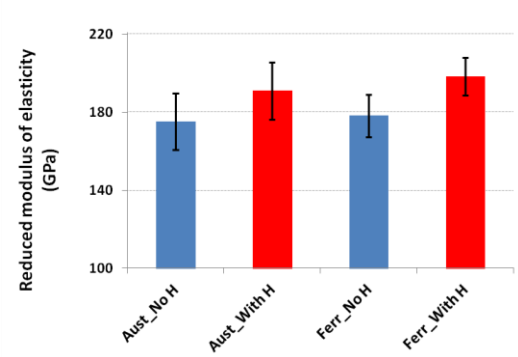

Fig. 9. The hydrogen effect on the reduced modulus of elasticity

The effect of hydrogen on the hardness is larger for the austenite than for the ferrite, the differences in hardness, before and after hydrogen charging, being of about 1 GPa for the austenite and of 0.6 GPa for the ferrite. A higher increase in the hardness for the austenite is due to a higher solubility of hydrogen in the austenite as comparing to the ferrite.

From Fig. 9, we can disregard the effect of hydrogen since the increase of the reduced modulus of elasticity is within the measurement error and it is not sure that is due to the presence of hydrogen.

Another effect of hydrogen evolved during the cathodic potential is on the onset of plasticity. Fig. 11 presents typical load displacement curves and the difference between the pop-in load levels, when the nanoindents are made with and without hydrogen. Since more than 30 nanoindentations were made for each phase and each testing condition in order to have repeatability, the pop-in event frequencies are presented in Fig. 10. A decreasing in pop-in load level was observed for both the austenite and the ferrite phases.

The elastic part of the load – displacement curves presented in Fig. 11 can be fitted to the Hertzian equation:

$$P = 1.33E_r h^{1.5}\sqrt{R} \tag{9}$$

Mechanical Testing and Diagnosis, ISSN 2247 – 9635, 2012 (II), Volume 2, 5-14

where: P - the applied load, h - the indentation depth, R - the radius of the indenter tip, E_r - reduced modulus of the sample, given by the Eq. (7).

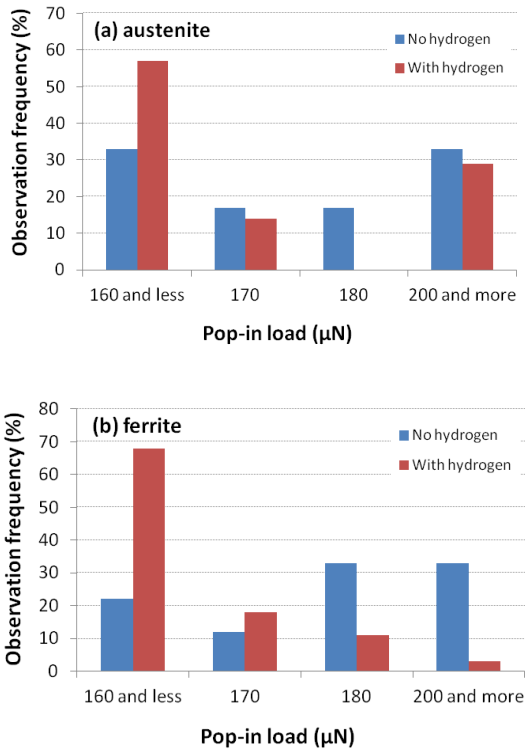

Fig. 10. Pop-in event frequencies for (a) austenite, (b) ferrite

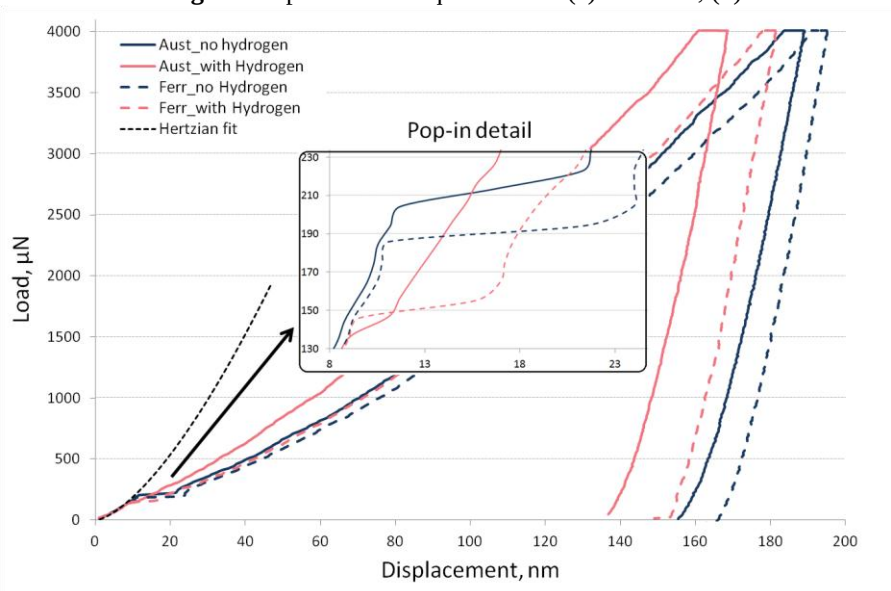

Fig. 11. The reduction in the onset of plasticity (pop-in load level) due to hydrogen

During a nanoindentation, the indenter tip will approach the sample with a certain velocity and as soon as the contact is established, the initial elastic loading begins until the first dislocation nucleation (or pop-in) occurs. The stress field underneath the indenter tip during the elastic deformation is described via continuum mechanics, assuming that the indenter tip is spherical [17]. When this assumption is made, the maximum shear stress under the indenter tip is:

$$\tau_{max} = 0.31\sqrt[3]{\frac{6E_r^{\,2}P}{\pi^3 R^2}} \tag{10}$$

According to continuum mechanics, the maximum shear stress occurs at a distance of approximately 0.48 times the contact radius, r_c, directly below the center axis of the contact, between the sample and the indenter tip [17]:

$$z_{\tau(max)} = 0.48\, r_c \tag{11}$$

If the contact radius between the indenter tip and the sample is [17]:

$$r_c = \frac{\pi R}{2E_r}\sqrt[3]{\frac{6E_r^{\,2}P}{\pi^3 R^2}} \tag{12}$$

replacing Eq. (12) in Eq. (11), the position of the maximum shear stress, $z_{\tau(max)}$ can be calculated as:

$$z_{\tau(max)} = 0.48\, r_c = 0.48\sqrt[3]{\frac{3PR}{4E_r}} \tag{13}$$

The maximum shear stress acting at the $z_{\tau(max)}$ is responsible for the homogeneous dislocation nucleation in the volume below the surface and is in the order of the theoretical strength of a defect free material, according to the Frenkel model [18]:

$$\tau_{th} \approx \frac{G}{2\pi} \approx \frac{G}{10} \tag{14}$$

where G is the shear modulus.

Now, we can equate the measured maximum shear stress during pop-in to the theoretical strength of the austenite or the ferrite phase in Eq. (14). This relates any change in the pop-in load to a change in the shear modulus of the given phase in SDSS as a result of hydrogen. In other words, hydrogen not only facilitates the dislocation nucleation, but also reduces the lattice cohesion [19].

A deeper analysis of the pop-in behavior was made using a pop-in finder program developed by Barnoush [14]. The program is using the load displacement curves imported from the Hysitron software and is finding the pop-in from the analysis of the regions where the displacement is constant. Further, based on the Hertzian fit, Eq. (9) the tip radius is found and used for calculating the position of the maximum shear stress and its value, Eq. (10) to (13).

Fig. 12 presents the decrease in both pop-in width and pop-in load for the austenite and the ferrite, in the presence of hydrogen. The pop-in i.e. homogeneous dislocation nucleation in the austenite requires higher load levels than the ferrite, but the width of the pop-in is smaller. The pop-in width in the austenite is reduced to half in the presence of hydrogen while for the ferrite, the decreasing is around one third.

Mechanical Testing and Diagnosis, ISSN 2247 – 9635, 2012 (II), Volume 2, 5-14

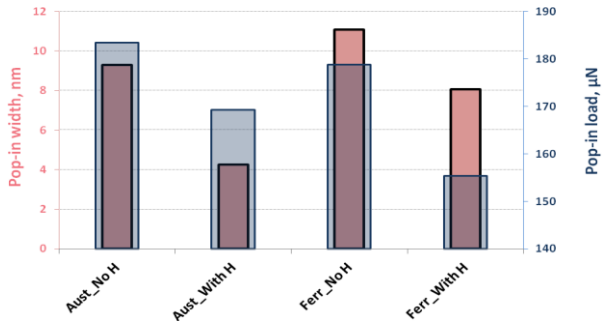

Fig. 12. Pop-in width and pop-in load from the pop-in analysis

Table 2 presents a summary of the nanomechanical properties of the SDSS, extracted from the load-displacement curves and from the pop-in finder program. The maximum shear stresses are higher when hydrogen is present in the material and closer to the surface. It should be mentioned that in the SDSS, in order to have both phases in quasi equilibrium with each other, it is necessary to quench them from about 1100°C down to the room temperature. This results in the formation of very high tensile stresses in the austenite and compressive stresses in the ferrite [20]. This is very important to consider the effect of these local high residual stresses on hydrogen uptake and its effect on the measured nanomechanical properties. Therefore, future works are planned to study the effect of hydrogen on the nanomechanical response of the austenite and the ferrite phases in combination with these residual stresses.

4. CONCLUSIONS AND FURTHER WORK

The increase in the hardness and the decrease in the pop-in load level of both the austenite and the ferrite phases were observed due to hydrogen evolution after the cathodic potential was applied to the sample. While the decrease in the pop-in can be related to the hydrogen effect on the interatomic potential, the cohesion the effect of hydrogen on hardness is in agreement with the hydrogen pinning effect on the dislocations.

Table 2. Summary of the nanomechanical properties of SDSS

	Load displacement curves			**Pop-in analysis**				
	H (GPa)	**Er (GPa)**	**S (µN/nm)**	**Start load (µN)**	**Start depth (nm)**	**Width (nm)**	**Maximum shear stress**	
							$z_{\tau(max)}$ **(nm)**	τ_{max} **(GPa)**
Austenite_air	5.1	175	176	183	10.8	9.3	31.1	2.90
Austenite_hydrogen	6.4	191	171	177	11.5	4.0	26.5	3.74
Ferrite_air	4.8	178	184	178	11.2	11	27.7	3.40
Ferrite_hydrogen	5.3	198	194	155	10.9	8.0	23.4	3.43

The Super Duplex Stainless Steel is a very complex material as well as is the hydrogen embrittlement micromechanism and further investigations have to be made. Further work will focus on the hydrogen effect on the grains with different crystallographic orientations. Also, different loading rates will be considered.

REFERENCES

1. **Troiano, A.R.**, 1960, The role of hydrogen and other interstitials in the mechanical behaviour of metals, *Trans ASM*, 52, pp. 54-80.
2. **Birnbaum H.K., Sofronis P.**, 1994, Hydrogen-enhanced localized plasticity-a mechanism for hydrogen-related fracture, *Materials Science and Engineering: A*, 176(1-2), pp. 191-202.
3. **Nilsson J.O.**, 1992, Super duplex stainless steels, *Material Science and Technology*, 8(8).
4. **Krauss G.,** 2005, Steels: processing, structure, and performance.
5. **Zakroczymski T., Owczarek E.,** 2002, Electrochemical investigation of hydrogen absorption in a duplex stainless steel, *Acta Materialia*, 50(10), pp. 2701-2713.
6. **Oltra R., Bouillot C., Magnin T.**, 1996, Localized hydrogen cracking in the austenitic phase of a duplex stainless steel, *Scripta Materiale*, 35(9), pp. 1101-1105.
7. **Johnsen R., Nyhus B., Wästberg S., Lauvstad G.O.**, 2007, New Improved Method For Hisc Testing Of Stainless Steels Under Cathodic Protection. Corrosion, paper no. 07496.
8. **Olden V., Thaulow C., Johnsen, R., Østby E., Berstad T.**, 2009, Influence of hydrogen from cathodic protection on the fracture susceptibility of 25%Cr duplex stainless steel - Constant load SENT testing and FE-modelling using hydrogen influenced cohesive zone elements. *Engineering Fracture Mechanics*, 76(7), pp. 827-844.
9. **Olden, V., Thaulow, C., Johnsen R., Ostby E.**, 2007, Cohesive zone modeling of hydrogen-induced stress cracking in 25% Cr duplex stainless steel. *Scripta Materialia*, 57(7), pp. 615-618.
10. **Oliver W.C., Pharr G.M**., 1992, An improved technique for determining hardness and elastic modulus. *J. Mater. Res.*, 7(6).
11. **Fang, T., Chang W., Tsai S.,** 2005, Nanomechanical characterization of polymer using atomic force microscopy and nanoindentation. *Microelectronics Journal*, 36(1), pp. 55-59.
12. **Barnoush A., Vehoff H.,** 2006, Electrochemical nanoindentation: A new approach to probe hydrogen/deformation interaction, *Scripta Materialia*, 55(2), pp. 195-198.
13. **Barnoush A., Vehoff H.**, 2008, In situ electrochemical nanoindentation: A technique for local examination of hydrogen embrittlement, *Corrosion Science*, 50(1), pp. 259-267.
14. **Barnoush A.,** 2008, Hydrogen embrittlement, revisited by in situ electrochemical nanoindentation, PhD Dissertation.
15. **Øverland M.**, 2007, Hydrogen induced stress cracking in super duplex stainless steel, Master thesis.
16. **Hysitron**, 2009, TI-750 Ubi User Manual NRL-M-201 r9.0.0609 (TriboScan 9.1).
17. **Johnson K.L.**, 1985, Contact Mechanics. Cambridge Press, pp. 85-95.
18. **Frenkel, J.**, 1926, Zur Theorie der Elastizitätsgrenze und der Festigkeit kristallinischer Körper, *Zeitschrift für Physik A Hadrons and Nuclei*, Springer Berlin / Heidelberg, 37: pp. 572-609.
19. **Barnoush A., Vehoff H.**, 2010, Recent developments in the study of hydrogen embrittlement: Hydrogen effect on dislocation nucleation, *Acta Materialia*, 58(16), pp. 5274-5285.
20. **Barnoush A., Zamanzade M., Vehoff H.,** 2010, Direct observation of hydrogen-enhanced plasticity in super duplex stainless steel by means of in situ electrochemical methods. *Scripta Materialia*, 62(5), pp. 242-245.